A geometric approach for filament winding pattern generation and study of the influence of the slippage coefficient

Article *in* Journal of the Brazilian Society of Mechanical Sciences and Engineering · November 2019

DOI: 10.1007/s40430-019-2083-2

CITATIONS
22

READS
2,466

4 authors:

Ingo Hermann Dalibor

6 PUBLICATIONS **101** CITATIONS

SEE PROFILE

Tales de Vargas Lisbôa

Leibniz Institute of Polymer Research

41 PUBLICATIONS **259** CITATIONS

SEE PROFILE

Rogério J. Marczak

Federal University of Rio Grande do Sul

149 PUBLICATIONS **624** CITATIONS

SEE PROFILE

Sandro Campos Amico

Federal University of Rio Grande do Sul

505 PUBLICATIONS **10,371** CITATIONS

SEE PROFILE

A geometric approach for filament winding pattern generation and study of the influence of the slippage coefficient

Dalibor, I. H. [a], Lisbôa, T. V. [*b,c], Marczak, R. J. [c], Amico, S. C. [a,c]

[a] PPGE3M, Federal University of Rio Grande do Sul.
Av. Bento Gonçalves, 9500. Porto Alegre - RS. CEP 915.01-970. Brazil.

[b] Mechanics and Composite Materials Department, Leibniz-Institut für Polymerforschung.
Hohe Straße 6, 01069 Dresden, Germany.

[c] PROMEC, Federal University of Rio Grande do Sul.
Rua Sarmento Leite, 425. Porto Alegre - RS. CEP 900.50-170. Brazil.

[*] Corresponding Author – **taleslisboa@daad-alumni.de** .

Abstract

A special feature of the Filament Winding (FW) process is known as *pattern*: diamond-shape mosaic that results from the sequence of movements of the mandrel and tow delivery-eye. One of the main factors to generate different patterns is the return path of the tow and, for a non-geodesic trajectory, the path depends on the friction between tow and mandrel. Aiming at a practical description of the FW process, a novel geometric approach on pattern construction is presented. Pattern generation, skip configurations and definitions of geodesic and non-geodesic trajectories in regular winding and return regions are described based on developed surfaces, residue classes and modular arithmetic. The influence of mandrel's length, mandrel's rotation angle, and variation of the winding angle in the return region are presented, for they are important parameters of the process. Examples of winding angle, mandrel rotation and non-geodesic path in cylindrical and non-cylindrical surfaces of revolution are shown and discussed.

Keywords: filament winding; slippage coefficient on return path; geodesic and non-geodesic trajectories; geometric based pattern generation.

Highlights

- A novel geometric approach on pattern generation;
- Formalism for the geometric proposal through developed surfaces, residue classes and modular arithmetic;
- Correlation between the return non-geodesic path and slippage coefficient for surfaces of revolution;
- Correlation between dwell and possible patterns and skips.

1 Introduction

Filament Winding (FW), a widespread manufacturing process for composite materials, is usually applied to the production of parts of revolution, such as tubes, shafts and pressure vessels [1, 2, 3, 4]. Albeit the relative simplicity, optimal parameters are not always obtained due to the lack of detailed knowledge of the process [5]. In FW, the tow is led by a delivery-eye moving in a parallel (or near parallel) direction to the rotation axis of the mandrel from one end to another and then backwards, so that two layers are simultaneously wound. The delivery-eye positions the tow in a particular

winding angle – angle between the tangent to the winding path and the axis of rotation – which is determined by the ratio of the mandrel's angular velocity and the longitudinal velocity of the delivery-eye. From the three winding modes: hoop, polar and helical, only with the first does not generate the pattern.

The pattern is the mosaic arrangement of diamond shapes formed on the periphery of the wound part. They are generated due to the repetitive and regular movement of the helical winding. Even with the same amount of material and nearly the same production time, different patterns may impact the components' mechanical response, depending on the loading. Rouseau et al. [6] have carried out an extensive study on the effect of the pattern, i.e. the degree of interweaving, on the damage behaviour of wound tubes under different loads. The pattern has been reported to influence internal pressure [7], [8], compressive strength [9], but not buckling behaviour [10]. The divergence may be caused by the algorithms used by a particular CAM software. Consequently, it becomes imperative to understand precisely the formation of the pattern in order to select a suitable one for each specific usage. A detailed description of the pattern generation is difficult to find in the literature.

The objective of this work is to introduce a novel concept applied to the FW process based on geometric aspects and the sequence of its main movements, aiming at providing practical and a straightforward approach to the process. The pattern generation, the influence of the return region and the slippage coefficient on the process are highlighted. The technique adopts developed surfaces of revolution, residue classes, modular arithmetic and differential geometry in order to present the concepts and to prove properties. A comparison with the procedure used in most of CAMs, based on the solutions of Diophantine equations [1, 11], is also shown. The novelty of the idea introduced herein relies on an alternative equation to govern pattern generation, which allows different patterns to be created based on the same parameters, such as number of tows and winding angle, which could not be achieved through the Diophantine approach [12].

The approaches available to create wound surfaces are based on Diophantine equations and their solutions, whereas the introduced methodology is based on modular arithmetic to obtain different solutions. Simple and general cases of pattern generation are presented and the process' characteristics are defined and discussed. The equations of geodesic and non-geodesic trajectories are demonstrated and applied to two examples: cylindrical and non-cylindrical surfaces of revolution. The required tow length, mandrel's rotation and additional length due to the return region as well as the variation of the winding angle in the non-geodesic path are also determined.

This paper is divided into five sections and one appendix. The second presents the geometric approach for the pattern generation. The third shows the determination of several parameters of the geodesic and non-geodesic trajectory on surfaces of revolution. The fourth is devoted to some results and discussion. At the fifth section, the conclusions are presented. The appendix presents the detailed algebraic manipulation of the equation that links the pattern and the possible dwells angles.

2 Pattern generation

2.1 The pattern and properties

Figure 1 shows examples of diamond-mosaic figures called *pattern*. Both were produced by using nearly the same manufacturing parameters, such as winding angle, mandrel's radius, number of tows on the periphery, etc. Due to the inherent properties of the process, an integer number of diamond-shape forms are developed in the periphery of the mandrel along the circumferential direction. This integer classifies the pattern, i.e., Figures 1 (a) and (b) have patterns '5' and '9', respectively. Furthermore, given the triangle congruences generated by diamond-shape forms, the same number of diamond-shape forms is observable in the mandrel's axial direction, inside a tow pitch of the helical path.

Each diamond of the pattern can be divided in two main triangles, as shown in Figure 2. The left and right sides

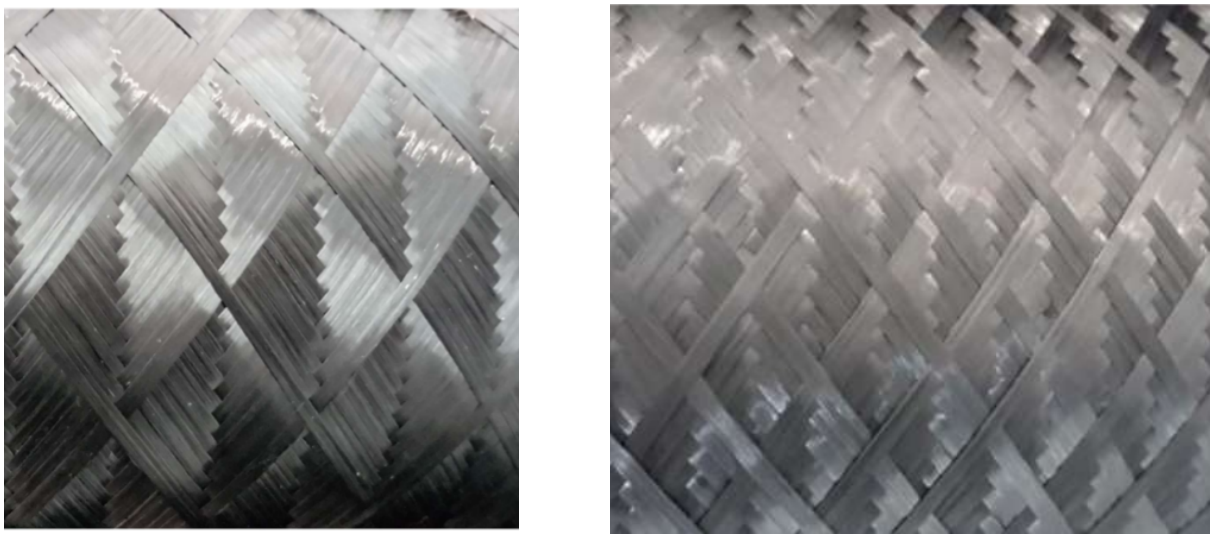

(a) (b)

Figure 1: Wound parts on the same mandrel with almost the same manufacturing parameters where (a) has 5 diamonds (with 9 tows in each diamond) and (b) has 9 diamonds (with 5 tows in each diamond) on the mandrel's periphery.

have winding angle $+\alpha$ and $-\alpha$ at the top surface, respectively. At the bottom (internal surface), the tow presents opposite winding angles. In each triangle, three different regions are identified as [9]: RL – the region similar to a regular antisymmetric laminated ply, CCO – the region influenced by the crossing of the tows in a zig-zag line, known as circumferential crossover circles, HCO – the region influenced by the outer borders called helical crossover circles. Moreover, in Figure 2, the dashed lines are divisions of an arbitrary diamond of the wound part and the solid lines define the actual entanglement region. In the HCO region, the lines define a tow centroid while in the CCO region, they determine the division of each triangle passing through the zig-zag region.

2.2 Developed surface and sequence of movements

A straightforward way to analyse pattern generation on cylindrical surfaces is to develop the surface of the mandrel into a rectangle, as shown in Figure 3. The horizontal and the vertical edges denote the component length and the circumference perimeter, respectively. Furthermore, the two horizontal edges are related to the same line in the cylinder, corresponding to 0° and 360° of the developed circumference. The tow width is initially neglected. Forward and backward strokes are presented in Figure 3 with solid and dashed lines, respectively. The direction of the tow placement is shown by the arrows. All of them have the same orientation (upwards) since the mandrel rotates to in one direction throughout the process. Each time the line reaches the superior limit, the trajectory starts again in the inferior one (developed surface + modular geometry). Figure 2 shows a laminate and the stacking of the left and right triangles of the diamond is a multiple of $[+\alpha/-\alpha]_n$ and $[-\alpha/+\alpha]_n$, respectively, where n is the number of the double laminae. Moreover, all the adjacent regions of a particular triangle has opposite stacking configurations.

In Figure 3, two regions are defined: regular winding and return region. In the former, the winding is regular and the tow follows a path to obtain the wanted winding angle. Normally, the path is geodesic in this region, which is the shortest trajectory between two points over a generic surface. Furthermore, on cylindrical surfaces, the winding angle of a geodesic path is constant. The geodesic path, however, is not mandatory for the process: it is only required that, at the same cross section, the forward and backward stroke have opposite winding angles in order to generate uniform surface and regular diamonds. In developed cylindrical surfaces, the geodesic paths are straight lines, easing the visualisation of the pattern generation. The second region – return region – is characterised by non-geodesic trajectories due to the return manoeuvre.

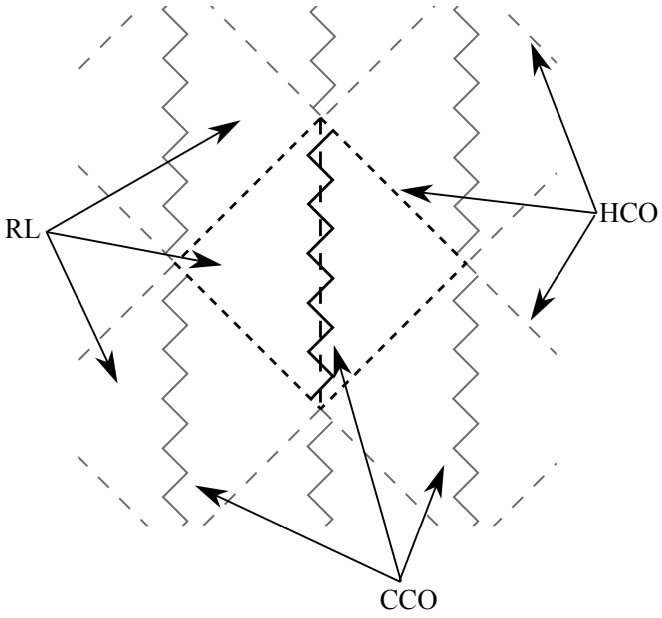

Figure 2: Scheme of the regions of the wound part.

The mandrel's rotation angle, performed during the return movement, is called *dwell* while a *circuit* is formed by two strokes (forward and backward) with their respective return paths. The set of circuits that take the tow to the adjacent position of the first forward stroke is a *cycle* and the number of circuits inside a cycle defines the pattern. The gaps between the tows, formed in the first cycle, are fulfilled in a sequential way. As the movements are repetitive and only complete circuits and cycles are performed, the way the filling occurs characterises the pattern by forming equal integral diamonds on the surfaces periphery.

Another movement in a cycle or at its end is known as *shift*: the displacement of the tow in the circumferential direction in order to prevent overlapping with an already deposited tow. This displacement is equal to the projection of the tow width onto the parallel direction. As a result, the shift, θ_{sft}, (measured in radians) is determined as

$$\theta_{sft} = \frac{w_p}{r},$$

in which

$$w_p = \frac{w}{\cos\alpha},$$

where w corresponds to the tow width, w_p to the projection of the tow width to the parallel direction and r defines the local radius of the surface of revolution. One notices that θ_{sft} also determines the section angle that a single tow occupies. The shift can be performed in a continuous way or it could be executed in a discrete fashion.

The continuous procedure does not require any modification of the velocity profile between the mandrel and the delivery eye throughout the process. It places the tow as described in refs. [1, 13, 14, 15] and it is suitable when there is no possibility of having an independent adjustment of the shift at the end of each cycle. This procedure is based on Bézout's identity [16] and, in this case, the number of tows, N, and the integer identifying the pattern, p_{tr}, are coprimes, resulting in

$$Na - p_{tr}b = \pm 1, \tag{1}$$

where $a, b \in \mathbb{Z}$ and b define the number of tows inside a diamond. The $\pm$ means that after p_{tr} circuits (a cycle), the tow will be positioned beside (before or after) the tow from the previous cycle. To determine a and b, the Euclidean algorithm may be applied [16].

The discrete procedure requires a different returning procedure at the end of each cycle. Thus, it is imperative that the relation between the delivery-eye velocity and the mandrel's rotation is modified in the middle of the process. Parameters

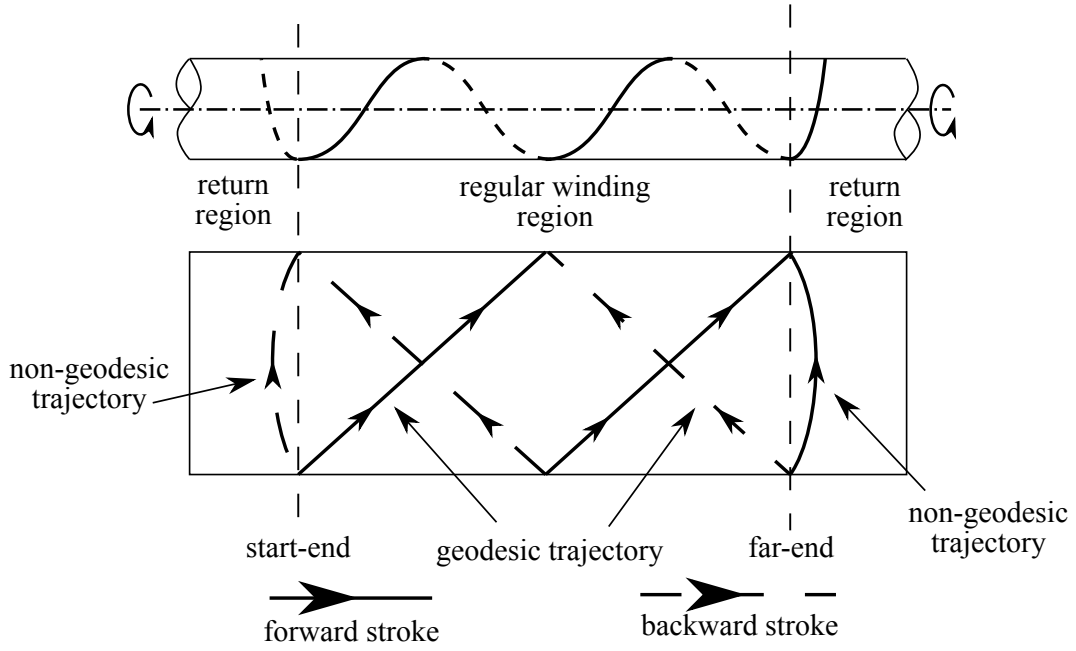

Figure 3: Scheme of a helical winding on a cylindrical mandrel.

such as winding angle are maintained. Nevertheless, small differences between the start-end and far-end return regions are expected.

2.3 Geometric approach with discrete shift

Regarding the helical pitch and the regular winding region and in order to ease the description of the introduced procedure, two cases can be considered: the first concerns one or multiple helical pitches that fit exactly on the component size, while the second represents a fractional helical pitch wound on the mandrel. These are described below.

First Case: L_r is a multiple of L

The first case is presented in Figure 4. L_r defines the pitch of the helical path and it represents twice the component length L. This basically means that the mandrel has to rotate twice (720°) until the tow travels from the start-end (A-A section) to the far-end (B-B section). The rectangle sides are the circumference perimeter, $2\pi r$, and the mandrel length, L_m, where r is the mandrel radius. In Figure 4, two circuits are presented, where the pattern is 1 ($p_{tr} = 1$), i.e., a cycle is complete after one circuit. In this case, the tow return trajectory close to the B-B section is generated in a full rotation of the mandrel. As a result, the b_1, first backward stroke, starts and ends at the same position as f_1. Such characteristic is shared for all forward f_i and backward strokes b_i, $i = 1, 2, \cdots, n$.

The shift may be defined as leading and lagging [11]. In the leading type, the shift is placed in the direction of the movement and, consequently, the dwell is slightly larger than the required for pattern generation (at B-B section). The lagging type is the direct opposite and the dwell is slightly smaller than the required for pattern generation. Figure 4 shows a leading type of shifting.

The described procedure is repeated until the mandrel is totally covered by the tows and some level of rounding is, hereby, required,

$$\left\lfloor \frac{2\pi r}{w_p} \right\rfloor \leqq N \leqq \left\lceil \frac{2\pi r}{w_p} \right\rceil , \tag{2}$$

where $\frac{2\pi r}{w_p} \in \mathbb{R}$ is the number of tows in order to cover fully the mandrel periphery. $\lfloor \cdot \rfloor$ and $\lceil \cdot \rceil$ correspond to the floor and ceil functions, respectively. Normally, the next integer is chosen (ceiling), wherewith there will be a small overlap,

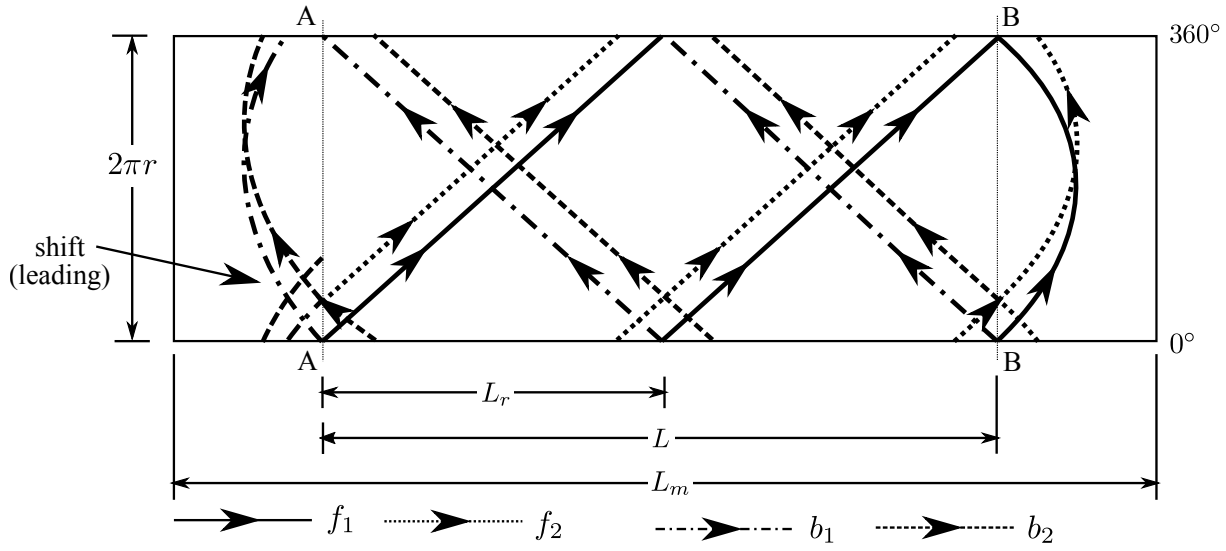

Figure 4: First case of pattern formation: pitch fits exactly the component length.

otherwise a small gap may occur. These small gaps may be filled with resin in the curing process. Equation (2) determines the number of tows required to achieve a minimum degree of gap or superposition. Other approaches may add / subtract tows so as to increase / decrease the degree of cover in orders larger / smaller than 100%.

In the case of Figure 4, the mandrel's rotation is a multiple of a full turn at the return region. However, this is not a requirement of the process. For instance, if $p_{tr} = 2$ has to be wound, as shown in Figure 5, the second forward stroke inside a cycle must be at 180° of the first one, at the A_2 position. The same circumferential distance must be ensured for the backward strokes: b_2 starts at B_3, which is located 180° from B_1, where b_1 starts. As a result, the dwell at each return region is 90°. The first circuit of the second cycle, represented by an arrowed solid line, would be placed at the same position of f_1, so a shift is performed.

Figure 6 schematically depicts a case with $p_{tr} = 5$. Circuits, c_i, are used instead of the strokes. The return trajectory takes 72° of the mandrel's rotation, thus the partitions P_i are shown with a spacing of 72°. The tow leaves the start end again at point A, arrives on the far end at point B and a dwell with 72° is done until point B_1. After a stroke, the tow arrives point A_1 at the start end, a dwell of 72° is performed and a new circuit begins at point A_2. After 5 times the tow is over the tow from the first cycle and a shift is performed and a new cycle begins. The sequence of the partition being fulfilled is: P_1, P_3, P_5, P_2 and P_4.

The dwell for a $p_{tr} = 5$ is not fixed at 72°. Indeed, the possible dwells are multiple of this value. The order of filling is, however, modified. The P_i sequences may be seen in Table 1 where s_{kp} is known as *skip* (as a partition is "jumped"): the ratio between the circumferential distance (anticlockwise) of two sequential strokes and the dwell. It is always an integer since this distance must be a multiple of the dwell.

Moreover, given the characteristics of a single circuit, the skip can be defined as

$$s_{kp} = \frac{2 d_w p_{tr}}{360} \,. \tag{3}$$

where d_w corresponds to the dwell. The factor 2 refers to the two return procedures inside a circuit. In Table 1, four examples of the sequence of circuits are presented.

Equation (3) may result in skip values larger than the pattern number and this is a consequence of the number of full rotations of the mandrel regarding the dwells. So, the skip can be viewed as a residue class, defined by $[s_{kp}]_{p_{tr}}$. So,

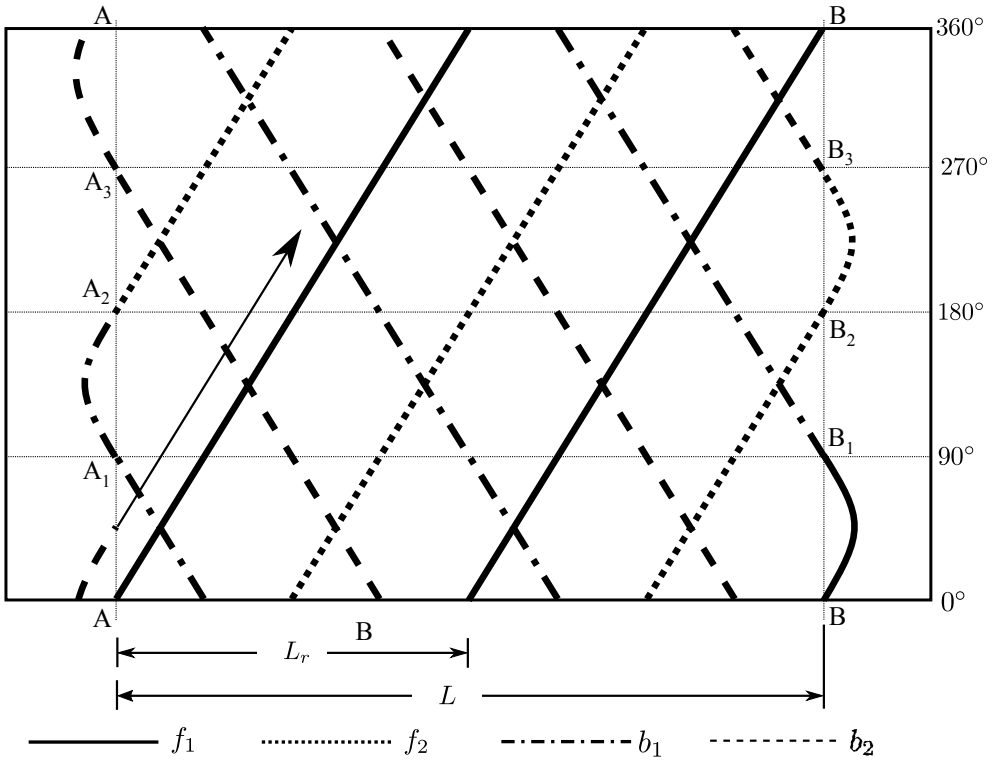

Figure 5: Scheme of tow placement and the dwell for a $p_{tr} = 2$.

Table 1: Example of different configurations for a pattern 5.

Dwell	Sequence of P_i	p_{tr} / s_{kp}
72°	1, 3, 5, 2, 4, shift, 1	5/2
144°	1, 5, 4, 3, 2, shift, 1	5/4
216°	1, 2, 3, 4, 5, shift, 1	5/1
288°	1, 4, 2, 5, 3, shift, 1	5/3

taking the aforementioned example of $p_{tr} = 5$, the classes are

$$
\begin{aligned}
[0]_5 &= \left\{\cdots \quad -10 \quad -5 \quad 0 \quad 5 \quad 10 \quad \cdots\right\} \Rightarrow p_{tr}/s_{kp} = 1/1\,, \\
[1]_5 &= \left\{\cdots \quad -9 \quad -4 \quad 1 \quad 6 \quad 11 \quad \cdots\right\} \Rightarrow p_{tr}/s_{kp} = 5/1\,, \\
[2]_5 &= \left\{\cdots \quad -8 \quad -3 \quad 2 \quad 7 \quad 12 \quad \cdots\right\} \Rightarrow p_{tr}/s_{kp} = 5/2\,, \\
[3]_5 &= \left\{\cdots \quad -7 \quad -2 \quad 3 \quad 8 \quad 13 \quad \cdots\right\} \Rightarrow p_{tr}/s_{kp} = 5/3\,, \\
[4]_5 &= \left\{\cdots \quad -6 \quad -1 \quad 4 \quad 9 \quad 14 \quad \cdots\right\} \Rightarrow p_{tr}/s_{kp} = 5/4\,,
\end{aligned}
$$

where each class generates a particular p_{tr}/s_{kp}. The class $[0]_5$ implies in $p_{tr}/s_{kp} = 1/1$ due to the fact that it leads to dwells multiple of 360°, obtaining a sequence of movements analogous to Figure 4.

Further properties on residue classes and modular arithmetic can be applied to p_{tr}/s_{kp} evaluation. A residue class is constructed by the well-known modular equation $a \equiv b \pmod{m}$. One important property regarding pattern development is when the modulo is a composite (non-prime) number: the entire equation can be reduced to another pattern. Let

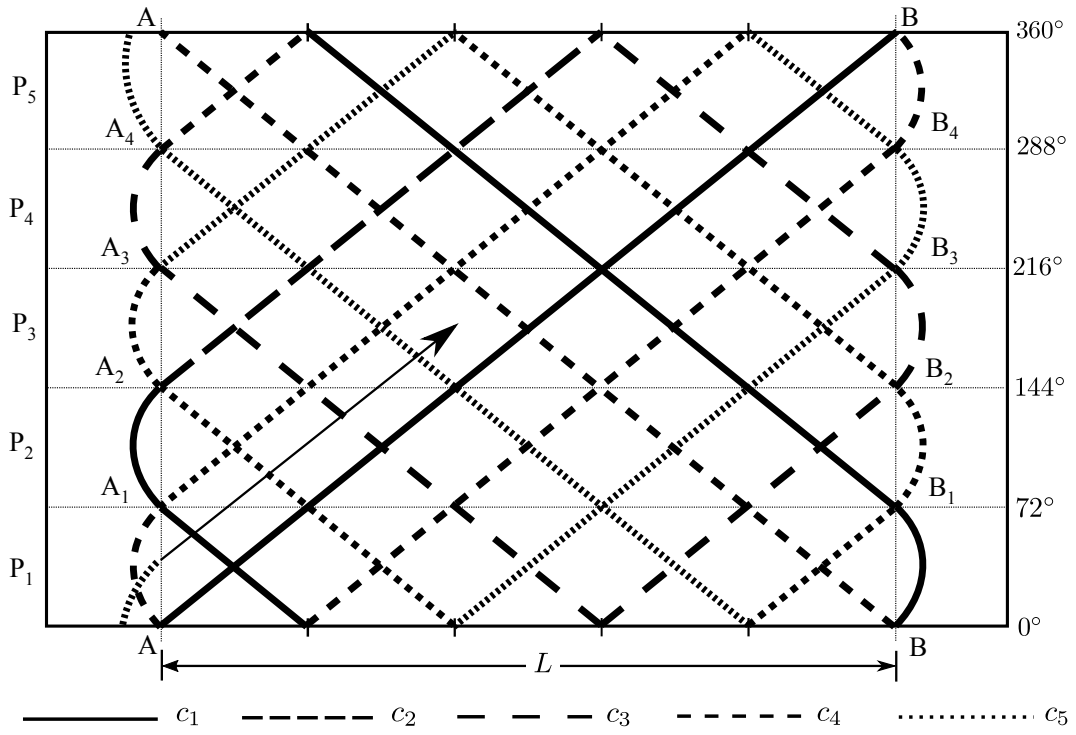

Figure 6: Fractional dwell at the first case of a pattern 5.

$p_{tr} = 4$, for example. Its residue classes are

$$
\begin{aligned}
[0]_4 &= \left\{\cdots \quad -8 \quad -4 \quad 0 \quad 4 \quad 8 \quad \cdots\right\} \Rightarrow p_{tr}/s_{kp} = 1/1\,, \\
[1]_4 &= \left\{\cdots \quad -7 \quad -3 \quad 1 \quad 5 \quad 9 \quad \cdots\right\} \Rightarrow p_{tr}/s_{kp} = 4/1\,, \\
[2]_4 &= \left\{\cdots \quad -6 \quad -2 \quad 2 \quad 6 \quad 10 \quad \cdots\right\} \Rightarrow p_{tr}/s_{kp} = 2/1\,, \\
[3]_4 &= \left\{\cdots \quad -5 \quad -1 \quad 3 \quad 7 \quad 11 \quad \cdots\right\} \Rightarrow p_{tr}/s_{kp} = 4/3\,.
\end{aligned}
$$

One notes that $p_{tr}/s_{kp} = 4/2 \Rightarrow p_{tr}/s_{kp} = 2/1$. This is a consequence of

$$ac \equiv bc \pmod{mc} \Rightarrow a \equiv b \pmod{m}\,, \tag{4}$$

and given the same implication, the class $[0]_{p_{tr}}$ always generates a $p_{tr}/s_{kp} = 1/1$. It is important to note that, as a corollary of eq. (4), every pattern construct by composite numbers has reductions. Only patterns with prime numbers has all skip configurations.

Another way to analyse the sequence of movements is depicted in Figure 7, where the order of tow placement is shown in the mandrel's cross section. In each Figure, 3 cycles are presented and the arrows define the tow sequence. In Figure 7 (a), the cycle starts at P_1, then goes to P_2 and continues anticlockwise until reaches P_1. A shift is performed and the next cycle starts. By observing Table 1, this pattern is classified as 5/1. Different orders of P_i can be considered. Figure 7 (b) presents a case in which a partition is skipped. The tow is placed at P_1, then goes to P_3 (skipping P_2) and to P_5 (skipping P_4). After, P_2 and P_4 are filled. In Table 1, this pattern is classified as 5/2. Thus, essentially, the skip can be assumed as the shift between two circuits inside a cycle, considering the partitions. The patterns 5/3 and 5/4 are also shown in Figure 7 (b) and (a), respectively, differing from 5/1 and 5/2 only through the clockwise sequence of fulfilling.

Figure 7 can also regarded as a fingerprint of a particular pattern / skip. Because of its modular properties, the reduction of patterns are naturally taken into account in this scheme. A wound part, regardless if it is cylindrical or not, presents such fingerprints.

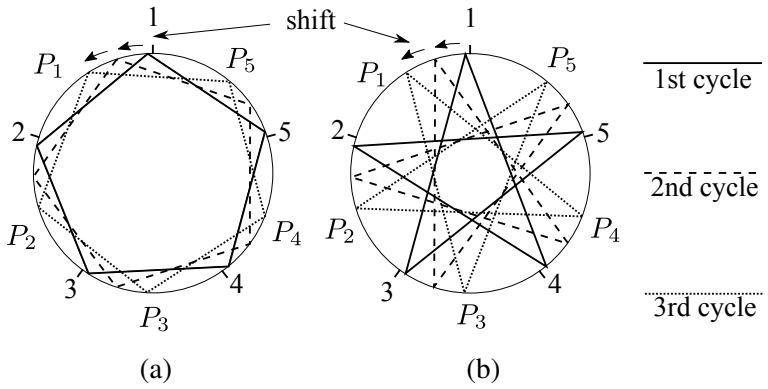

Figure 7: Different form of viewing the pattern formation.

As the pattern number increases, the distance between the zig-zag lines decreases (CCO regions in Figure 2) [17]. One can determine this distance as

$$d_{\mathrm{CCO}} = \frac{L_r}{2p_{tr}} \, . \tag{5}$$

d_{CCO} is a main winding parameter and depends on the radius of the mandrel only, r, and winding angle α. When L_r fits an integer number of times into L and assuming a dwell of 360° at both returning regions (besides the shift close to the start-end), only $p_{tr} = 1$ is possible and d_{CCO} is the largest possible, i.e. the RL region is the greatest possible. In ref. [6], the area ratio of the CCO region to the total diamond region were associated with weeping effects and crack propagation.

Independently of the sequence, the tows are placed side by side, regardless of the small overlap or gap due to the rounding. As shown in Figure 6, the starting point on A-A section, and the subsequent point at which the tow arrives at the B-B section defines all possible positions. The N positions may be divided into P_i partitions with equal number of tows, N_p. Thus

$$\frac{N}{p_{tr}} = N_p \, , \tag{6}$$

where only positions defined by an integer number of tows are permitted. Each tow position, t_j is defined through

$$t_j = j w_c \leq N \, , \tag{7}$$

in which $j \in \mathbb{N}$. In an example, $N = 40$ means that only 40 tows may be placed side by side in the equator (the largest diameter of the mandrel). Equation (6) infers another characteristic of the discrete approach, when comparing with the continuous one, as it modifies eq. (1) by the following

$$Na - p_{tr} N_p = 0 \, . \tag{8}$$

The variable a was added to eq. (6) to account for degrees of coverage larger or smaller than 100% [11].

Second Case: L_r is not a multiple times in L

In the second case, the pitch does not fit exactly the regular winding region, as schematically depicted in Figure 8. Both the fractional parts a_l and a_r, concerning the longitudinal and circumferential directions, are shown at the regions between A-A and A'-A' sections as well as B-B and B'-B' section, respectively. The region of exact fitting is centralised, although it is neither a requirement nor a simplification of the problem. Two circuits are shown (c_1 and c_2).

The dwell required to construct a particular pattern depends only on the fractional part and the dwell and not on the wound part of A'-A' to B'-B' sections (integer pitch). In order to prove such statement, let the mandrel's rotation in a single circuit be defined (in degrees) as

$$\theta^{circ} = 2 \left(360 \left\lfloor \frac{L}{L_r} \right\rfloor + 360 \frac{a_l}{L_r} + d_w \right) \, . \tag{9}$$

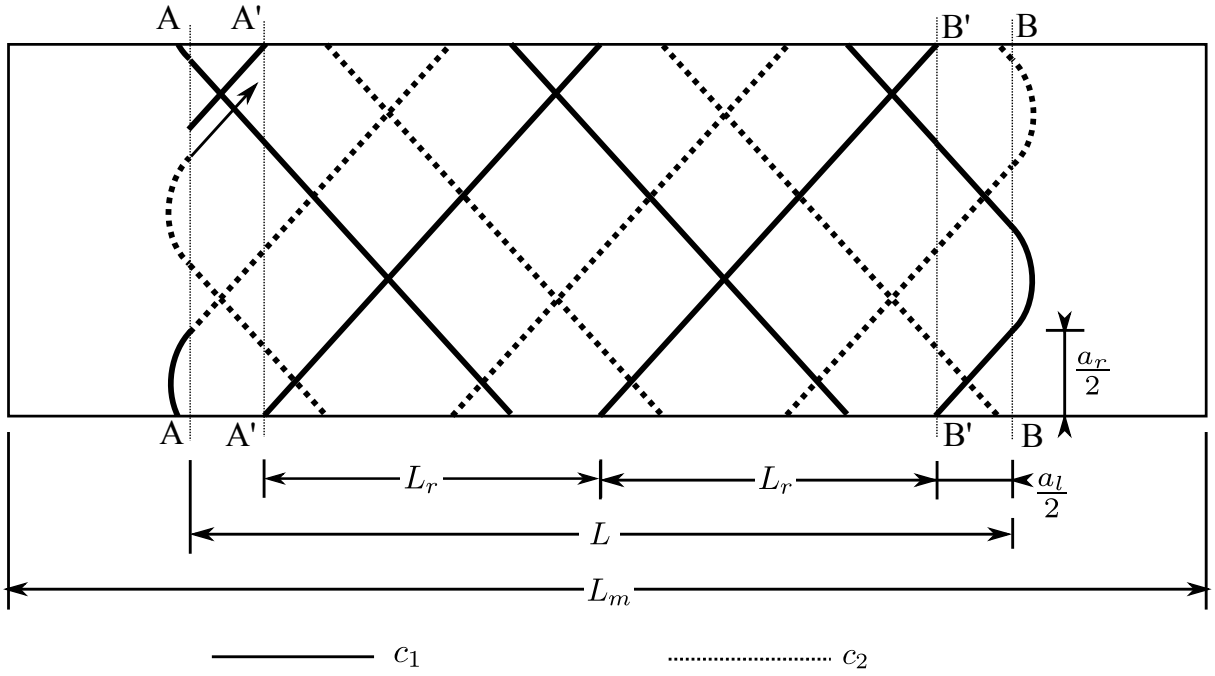

Figure 8: Fractional fitting.

Now, let

$$\hat{d}_w = 360\frac{a_l}{L_r} + d_w \,, \tag{10}$$

be a modified dwell due to the non fitting of the pitch in L. As aforementioned, the mandrel's rotation of a cycle is always a multiple of a full rotation. Otherwise, there would be no need to perform the discrete shift each time a cycle ends. Consequently,

$$p_{tr}\theta^{circ} = \theta^{cycle} = 360n_v \;\Rightarrow\; p_{tr}\theta^{circ} \equiv 0 \pmod{360} \tag{11}$$

as the number of rotations, n_v, is not important for pattern generation. By inserting eq. (9) into eq. (11) and performing algebraic manipulations described in Appendix A, one obtains

$$p_{tr}\hat{d}_w \equiv 0 \pmod{180} \tag{12}$$

Equation (12) establishes the required dwells, both modified and standard, given a particular pattern (or the possible patterns with respect to a dwell range). One notices that the possible patterns are defined by the number of tows, eq. (2), and, as a result, the winding angle. All properties introduced in the previous section remain the same, but the modified dwell. For exact fitting (first case), $\hat{d}_w = d_w$.

3 Non-geodesic trajectory on surfaces of revolution

Non-geodesic trajectories rely on the friction between mandrel and tow. These trajectories are required in the return region, since the winding angle changes from regular ($+\alpha$) to 90° and back again to regular but in the opposite direction ($-\alpha$).

3.1 Cylindrical Surfaces

An example of the previous section has assumed that the four dwell angles (72°, 144°, 216° and 288°) are theoretically possible for $p_{tr} = 5$. However, the dwell angle is a result of the non-geodesic path performed during the return procedure.

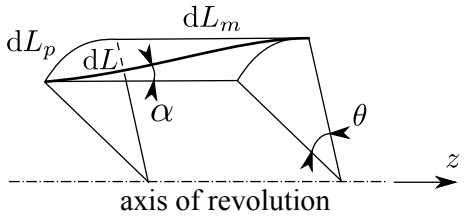

Figure 9: Infinitesimal revolution surface

In order to obtain the required rotation angle for a non-geodesic path over a cylindrical surface, an infinitesimal surface of revolution area has to be analysed, as depicted in Figure 9. Thus, let is consider a generic curve $\mathrm{d}L$, where $\mathrm{d}L_m$ and $\mathrm{d}L_p$ are the meridional and the parallel lengths, respectively. The radius of the surface of revolution, r depends only on the direction of the axis of rotation, z.

Through differential geometry [18]

$$\begin{aligned} \mathrm{d}L_m &= \sqrt{E}\mathrm{d}z \,, \\ \mathrm{d}L_p &= \sqrt{G}\mathrm{d}\theta \,, \end{aligned} \tag{13}$$

where E and G denote the coefficients of the first fundamental form of a surface. For revolution surfaces, they are determined as

$$\begin{aligned} E &= (r')^2 + 1 \,, \\ G &= r^2 \,, \end{aligned}$$

where the prime symbol indicates derivative with respect to z. The case of cylindrical surfaces reduces to

$$\begin{aligned} \mathrm{d}L_m &= \mathrm{d}z \,, \\ \mathrm{d}L_p &= r\mathrm{d}\theta \,, \end{aligned}$$

Through trigonometric relations, one obtains

$$\mathrm{d}L = \frac{\mathrm{d}z}{\cos\left(\alpha\left(z\right)\right)} = \frac{r\mathrm{d}\theta}{\sin\left(\alpha\left(z\right)\right)} \Rightarrow r\mathrm{d}\theta = \tan\left(\alpha\left(z\right)\right)\mathrm{d}z \,, \tag{14}$$

The differential equation of the winding angle variation on z-axis taking into account the slippage coefficient λ on a generic surface is written [19, 20] as

$$\frac{\mathrm{d}\alpha}{\mathrm{d}z} = \lambda\left[\frac{\sin\alpha\tan\alpha}{r} - \frac{r''\cos\alpha}{1+(r')^2}\right] - \frac{(r')^2\tan\alpha}{r} \,, \tag{15}$$

where the dependences of α on z is omitted. The slippage coefficient λ is obtained through the equilibrium condition [19] and it corresponds to

$$\lambda = \left|\frac{K_G}{K_N}\right| \,,$$

where K_G and K_N denote the geodesic and normal curvatures, respectively. The slippage coefficient has to be equal or lower than the friction factor to prevent slippage of the tow over the surface. Sometimes, a small increase in the friction coefficient reduces the returning path, enables a particular a pattern without additional rotations.

For cylindrical surfaces, with constant radius, eq. (15) is reduced to simple case as follow

$$\frac{\mathrm{d}\alpha}{\mathrm{d}z} = \lambda\frac{\sin\alpha\tan\alpha}{r} \,, \tag{16}$$

One notes that eq. (15) describes a non-geodesic path on a cylindrical surface. A geodesic trajectory is obtained considering the slippage coefficient null. In this case, the solution degenerates to the Clairaut relation, defined by

$$r\sin\alpha = c \,,$$

where c is a constant. The general solution of eq. (16) is

$$\frac{\sin(\alpha)-\sin(\alpha_i)}{\sin(\alpha)\sin(\alpha_i)}=\frac{\lambda}{r}(z_f-z_i) \quad \Rightarrow \quad \sin(\alpha)=\frac{\sin(\alpha_i)}{1-\dfrac{\lambda(z-z_i)\sin(\alpha_i)}{r}}\,, \tag{17}$$

where α_i and α are the initial and final winding angles with their respective positions, z_i and z. From eq. (17), one can determine the position where the tow changes the stroke (forward to backward and *vice-versa*), z_f, considering $\alpha=\alpha_f=90^\circ$ [17]. This information is important as it defines the required (minimum) mandrel length.

Along with eq. (17), one obtains the half-length of the tow required for the return procedure by integrating eq. (14). For integration purposes, let

$$a=\sin(\alpha_i) \quad b=\frac{\lambda}{r} \quad \mu=1-abz\,. \tag{18}$$

and considering $z_i=0$, this leads to

$$z_f=\frac{1-a}{ab}\Rightarrow \mu_f=a\,. \tag{19}$$

Equation (19) measures the required length to the returning path along the z-axis. The integrations are carried out over μ, thus the Jacobian is

$$\frac{\mathrm{d}\mu}{\mathrm{d}z}=-ab\,.$$

By inserting eq. (17) into eq. (14), one obtains

$$\mathrm{d}L=-\frac{1}{ab\cos\left(\arcsin\left(\dfrac{a}{\mu}\right)\right)}\mathrm{d}\mu=-\frac{\mu}{ab\sqrt{\mu^2-a^2}}\mathrm{d}\mu\,, \tag{20}$$

and, therefore,

$$\int_0^{L(\mu)}\mathrm{d}L=-\int_{\mu_i}^{\mu}\frac{\mu}{ab\sqrt{\mu^2-a^2}}\mathrm{d}\mu\,. \tag{21}$$

The integration of eq. (21) results in

$$L(\mu)=\frac{1}{ab}\left[\frac{\left(a^2-\mu^2\right)}{\sqrt{\mu^2-a^2}}-\frac{\left(a^2-1\right)}{\sqrt{1-a^2}}\right]\,, \tag{22}$$

where $\mu_i=1$ ($z=0$). Equation (22) is indeterminate for $\mu=a$ since $\tan\alpha\to\infty$ at the turning point. Applying the L'Hopital rule, with $\mu\to a$, eq. (22) yields

$$L(a)=\frac{\left(1-a^2\right)}{ab\sqrt{1-a^2}}\,. \tag{23}$$

Equation (23) defines the half-length of the return path and two limits may be identified. Firstly, if the initial angle is close to 90° as in hoop winding, the length is the smallest possible ($a\approx 1$). Finally, if $\alpha\approx 0^\circ$, the half-length required tends to infinity.

Another important parameter is the dwell, θ, for the half-length L (eq. (23)). Firstly, one considers eq. (14) along with eqs. (17) and (18) to write

$$r\int\mathrm{d}\theta=-\frac{1}{ab}\int\tan\left(\arcsin\left(\frac{a}{\mu}\right)\right)\mathrm{d}\mu\,,$$

which results in

$$\theta(\mu)=\frac{1}{\lambda}\ln\left|\frac{\sqrt{\mu^2-a^2}-\mu}{\sqrt{1-a^2}-1}\right|\,. \tag{24}$$

An interesting point of the eq. (24) is that the half-dwell does not depend on the mandrel radius, which is obtained by

$$\theta(a)=\frac{1}{\lambda}\ln\left(\frac{a}{1-\sqrt{1-a^2}}\right)\,.$$

3.2 Non-cylindrical surfaces of revolution

In order to determine non-geodesic trajectories on generic surfaces, a position vector, $\mathbf{d}$, is defined as

$$\mathbf{d}\,(z)^{\mathrm{T}} = \left\{ r\cos\theta \quad r\sin\theta \quad z \right\}^{\mathrm{T}} , \tag{25}$$

where r depends only on z. Differentiating $\mathbf{d}$ with respect to z, one obtains

$$\mathbf{d}'^{\mathrm{T}} = \left\{ r'\cos\theta - r\theta'\sin\theta \quad r'\sin\theta + r\theta'\cos\theta \quad 1 \right\}^{\mathrm{T}} , \tag{26}$$

in which the dependence of $\mathbf{d}'$ on z is omitted.

The angle between the $\mathbf{d}'$ and $\hat{\mathbf{e}}_z$ $\left(= \left\{ 0 \quad 0 \quad 1 \right\}\right)$ vectors defines the winding angle α, written as

$$\mathbf{d}' \cdot \hat{\mathbf{e}}_z = \left|\mathbf{d}'\right| |\hat{\mathbf{e}}_z| \cos\alpha \quad \Rightarrow \quad \cos\alpha = \frac{1}{|\mathbf{d}'|} . \tag{27}$$

Considering that the norm of $\mathbf{d}'$

$$\left|\mathbf{d}'\right| = \sqrt{r'^2 + r^2\theta' + 1} , \tag{28}$$

one derives the mandrel's rotation by the following differential equation

$$\theta' = \frac{\sqrt{\tan^2\alpha - r'^2}}{r} \tag{29}$$

which is obtained by algebraic manipulation of eqs. (27) and (28). Equation (29), along with eq. (15), determine the mandrel's rotation and the winding angle through a generic revolution surface. Therefore,

$$\mathbf{H}'\,(z) = \begin{Bmatrix} \theta'(z) \\ \alpha'(z) \end{Bmatrix} \Rightarrow \mathbf{H}\,(z) = \begin{Bmatrix} \theta(z) \\ \alpha(z) \end{Bmatrix} , \tag{30}$$

Given the characteristics of $\mathbf{H}'\,(z)$, θ and α can only be obtained by a numerical procedure. Thus, the non-geodesic path over a generic surface of revolution may be determined.

4 Results and discussion

The proposed geometric approach with discrete shifting is applied to the pattern generation and compared with the usual continuous procedure in the possible patterns which each can generate. Furthermore, the algorithm of the proposed approach is implemented in a CAD software and some results of the proposed approach are shown. The geodesic and non-geodesic trajectories, both in cylindrical and non-cylindrical surfaces are also demonstrated and used to determine the minimal dwell for a given slippage coefficient, which is useful for manufacturing and determines the pattern generation. Then, by using the possible patterns and the minimum dwell angle, some examples are provided to show the influence of patterns / skips on the the processing variables such as material used and minimum mandrel's size. The parameters varied at the examples are the radius, winding angle and the tow width.

4.1 Comparison between methods (Diophantine equation $\times$ geometric approach) regarding the possible patterns

Two different configurations are chosen for the comparison between the sets of patterns generated by the Diophantine and geometric approaches:

1. $r = 25$ mm, $w = 2$ [mm] and $\alpha = 60°$;

2. $r = 25$ mm, $w = 6$ [mm] and $\alpha = 45°$.

By considering eq. (2), it is noticeable that the number of tows in the mandrel's periphery will change and this will lead to different possible patterns. When considering the smallest gap or superposition, the number of tows, N, with winding angle equal to $60°$ is 39 and 40, respectively. Tables 2 and 3 present the values of the patterns considering the Diophantine equation (eq. (1)) and the geometric approach (eq. (8)), respectively. For the case of winding angle equal to $45°$, $18 \leqq N \leqq 19$. Similarly to the previous case, the possible patterns are shown for each procedure in Tables 4 and 5.

Table 2: Patterns obtained by the solution of the diophantine equation with a winding angle equal to $60°$.

N	40								39										
p_{tr}	1	3	7	9	11	13	17	19	1	1	2	4	5	8	10	19	7	14	16
a	1	1	3	2	3	1	3	9	1	1	1	1	1	1	1	1	2	5	7
b	39	13	17	9	11	3	7	19	40	38	19	10	8	5	4	2	11	14	17

Table 3: Patterns obtained by the geometric approach with a winding angle equal to $60°$.

N	40							39		
p_{tr}	1	2	4	5	8	10	20	1	3	13
N_p	40	20	10	8	5	4	2	39	13	3

Table 4: Patterns obtained by the solution of the diophantine equation with a winding angle equal to $45°$.

N	19					18		
p_{tr}	1	2	3	4	7	1	5	7
a	1	1	1	1	3	1	2	2
b	18	9	6	5	8	17	7	5

The patterns of Tables 2 and 4 where $a \neq \pm 1$ may not be easily distinguishable due to the diamonds entanglements. Moreover, similar patterns with different a values result in distinct laminates, with a possible influence on their mechanical properties. As can be seen in Table 2, only three patterns for $N = 40$ and eight patterns for $N = 39$ are considered with $a = \pm 1$. Moreover, with $N = 39$, more solutions of eq. (1) are obtained due to the fact that N has less divisors. The opposite is observed for the geometric approach with discrete shifting (Tables 3 and 5). The more divisors the N has, the more patterns are possible. It is important to notice that the list given in Table 3 considers only values for $a \neq 1$ for the same reason as the continuous approach.

In the second case, an interesting result is obtained. Considering superposition, $N = 19$ is a prime number. So, the only pattern possible in the geometric approach is $p_{tr} = 1$, as shown in Table 5. Nevertheless, as discussed in section 2.3, by the geometric approach, only N prime has all skips. In other words, the set p_{tr}/s_{kp} does not fall into another configuration.

Along with the sequence of movements described in section 2.2, the algorithm of the geometric approach is then implemented in a CAD / CAE software. The results for the cases of $N = 40$ and $N = 39$ (winding angle equal to $60°$) are depicted in Figure 10 for two different patterns each. The three regions depicted in Figure 2 are noticed in Figure 10 (a)-(d). As one can see, the pattern is generated without gaps and, most importantly, for cases which are not possible by the usual procedure.

One important property of the new approach is its simplicity as defines the possible patterns by just analysing the divisors of the number of the tows. Higher degrees of superposition / gap can be also evaluated by exactly the same

Table 5: Patterns obtained by the geometric approach with a winding angle equal to $45°$.

N	19	18				
p_{tr}	1	1	2	3	6	9
N_p	19	18	9	6	3	2

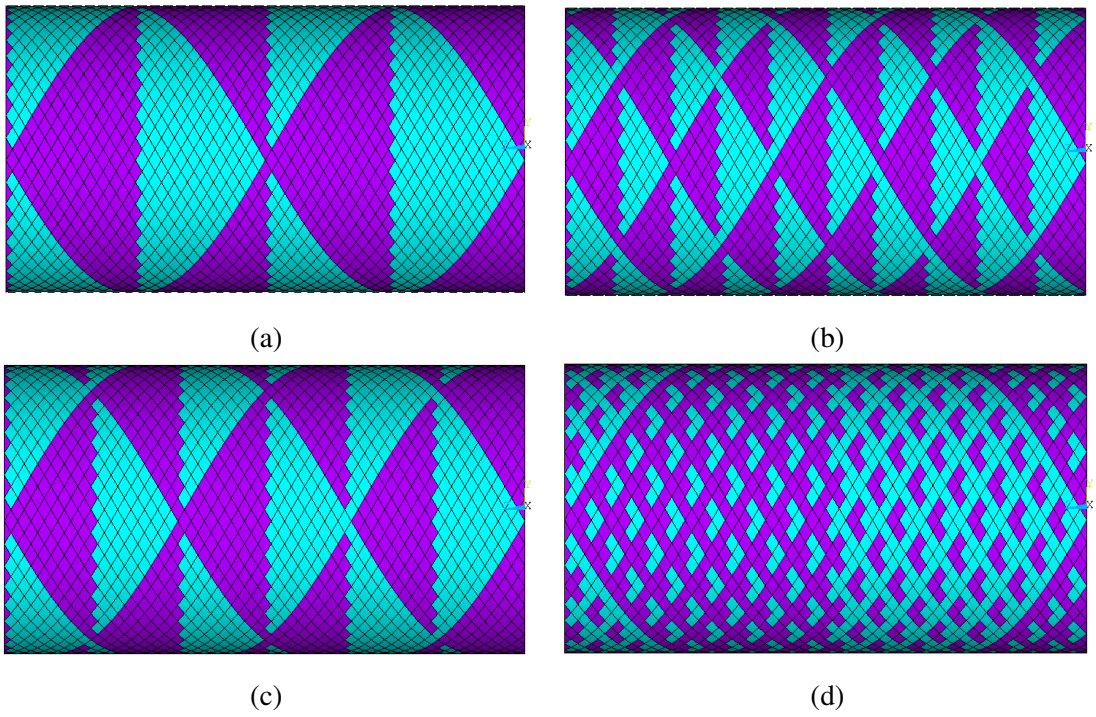

Figure 10: Pattern generated by the geometric approach with parameters (a) $N = 40$ and $p_{tr} = 2$, (b) $N = 40$ and $p_{tr} = 5$, (c) $N = 39$ and $p_{tr} = 3$ and (d) $N = 39$ and $p_{tr} = 13$.

manner. An example is the case of winding angle equal to $45°$. With 19 tows – considering superposition, one can only produce 1 pattern. If one increases one tow from the set, thus $N = 20$, one can then produce 5 different patterns. The degree of coverage is $\approx 102.82\%$ and $\approx 108.04\%$ for $N = 19$ and $N = 20$, respectively. It is also worthwhile noticing that, by the same way of varying the winding angle, if one changes the radius, the tow width and / or the degree of superposition / gap, the number of tows will change, implying in a modification of the possible patterns.

It is worth to highlight in Tables 2 - 5 that only $p_{tr} = 1$ is obtainable by both approaches. No other pattern obtained by the geometric approach can be obtained with the Diophantine equations. This occurs since N and p_{tr} need to be co-primes in the Diophantine approach, but they only need to be divisible for the geometric one. Another interesting consequence is that the cases that the Diophantine equations generate less possibilities are those where the geometric approach generates more. This is a valuable outcome because it brings the formalism closer to the manufacturing parameters and allows the construction of other patterns just by changing the rules of their generation. As aforementioned, one may change the number of tows to produce other patterns. This, however, directly impacts the degree of coverage and, as a consequence, thickness of the wound component.

4.2 Non-geodesic trajectory

Cylindrical surface of revolution

Trajectories, winding angle and mandrel's rotation at the return region on cylindrical and surfaces of revolution are discussed here. Firstly, concerning cylindrical surfaces, eq. (24) is plotted in Figure 11 for four different slippage

coefficients ($\lambda = 0.1$, $\lambda = 0.2$, $\lambda = 0.3$ and $\lambda = 0.4$), where z and θ correspond to the the additional mandrel size and rotation, respectively, at the returning region. If the slippage coefficient of the mandrel is 0.1, for example, the shortest trajectory that would prevent slippage of the tow in the return path is presented by the curve with solid circles. This represents $640°$ of rotation – almost two turns – only for the tow to return to the regular winding region. It can be observed that greater rotation and longer trajectories are needed, increasing the amount of material that will later be removed to reveal the part. Figure 11 also implies that the larger the slippage coefficient, the smaller the mandrel's rotation θ and the required size of the return region. Moreover, accordingly to eq. (24) for $\lambda = 0.1$, ca. 40-mm long return size is required, while for $\lambda = 0.2$, this length drops to ≈ 20 mm, which will also impact overall minimum mandrel length. It is worth noticing that these curves represent the minimum values that can be obtained without slippage and help defining the returning trajectory of a component for a particular pattern, as will be shown later.

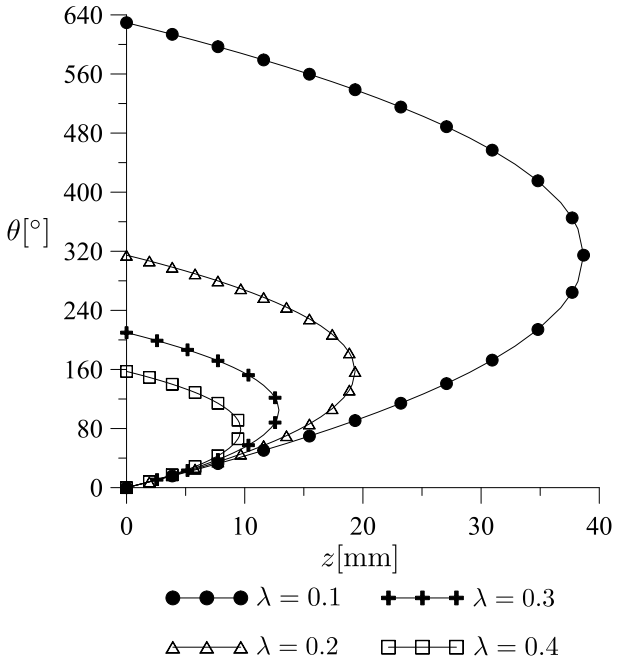

Figure 11: Non-geodesic path in the return region at the ends of the mandrel for different slippage coefficients ($r = 25$ mm).

The plots in Figure 12 (a)-(b) show the correlation between selected manufacturing parameters: mandrel's rotation, slippage coefficient, stroke, z_f, and the winding angle (of the regular winding region), α_i, at the return region. These results also represent the minimum bounds for these parameters or relations. One may notice that, as $\lambda \to 0$, the required mandrel's rotation (Figure 12 (a)) and mandrel's length for the return manoeuvre tends to infinity, independently of the winding angle. A similar trend is noted as the winding angle tends to $0°$, as mentioned before. Also, the closer the initial winding angle is to $90°$, the shorter is the return path.

Non-cylindrical surface of revolution

An example of a non-geodesic path is depicted in Figure 13 for the winding angle and the mandrel's rotation in a non-cylindrical surface of revolution governed by

$$r = 5.573110^{-6} z^3 - 0.00226208 z^2 + 0.480329 z + 17.9 \ \ [\text{mm}]\,, \tag{31}$$

where $z_i = 0$ mm and $z_f = 108$ mm. Its generatrix is plotted in Figure 14. The winding angle at z_i is $55°$. The winding angle and the mandrel's rotation governing equations (eq. (30)) are solved with a Runge-Kutta algorithm – RK4 – with 1500 points. Five slippage coefficients are evaluated. Interestingly, the winding angle for $\lambda = 0.4$ decreases until $\approx 40°$

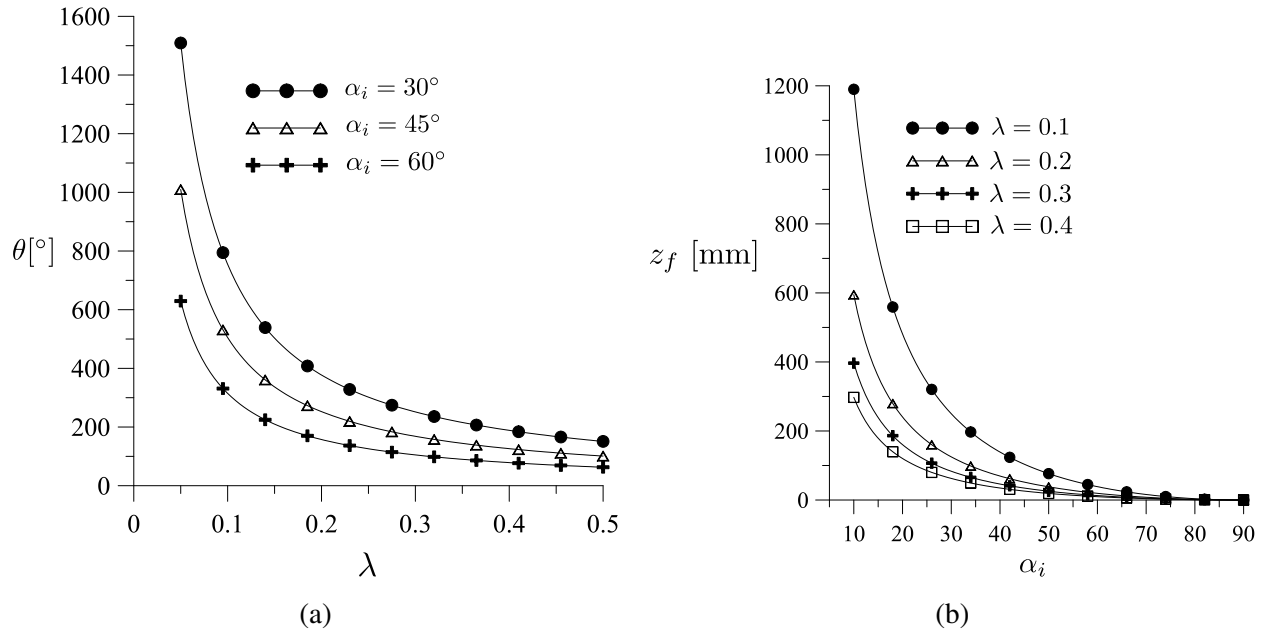

Figure 12: Bounds for the return region: (a) return angle $\times$ slippage coefficient for different winding angles and (b) length of return stroke $\times$ winding angle for different slippage coefficients.

and then increases to the initial winding angle. The same trend is found for $\lambda = 0.5$, but due to the high friction between the tow and the mandrel, the trajectory has a return ($\alpha = 90^\circ$) before the end of the mandrel, at $z \approx 72$ mm. This behaviour is similar to the non-geodesic trajectories in cylindrical surfaces previously shown in Figure 11.

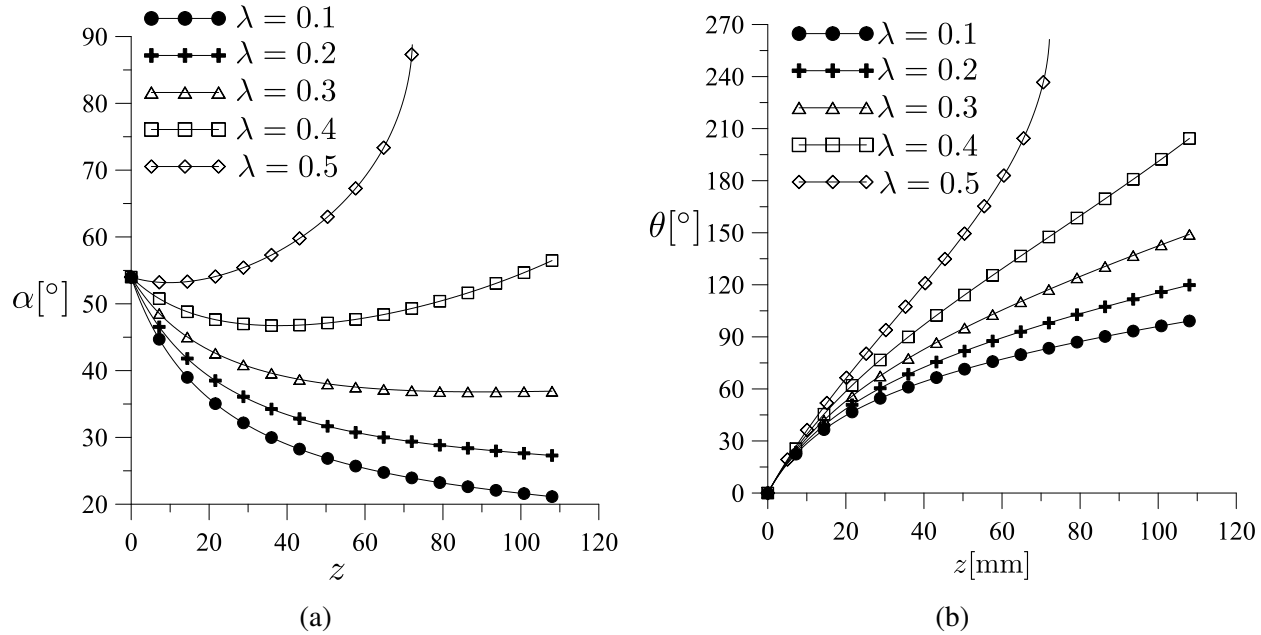

Figure 13: (a) Winding angle $\times$ stroke and (b) mandrel's angle $\times$ stroke at the return region for a non-cylindrical revolution surface.

Here again, these are the maximum bounds for the trajectories without slippage. For a friction between mandrel and tow of $\lambda = 0.5$, for example, any trajectory presented in Figure 13 (a) and the geodesic case can be generated without slippage. These results enable prediction of a path that fully covers the component surface as well as the initial angle of the returning region, whose relevance is evident from Figure 12. If the returning region of the component of Figure 14 is a cylinder and $\lambda = 0.2$, for example, the additional mandrel's length is larger than the component itself.

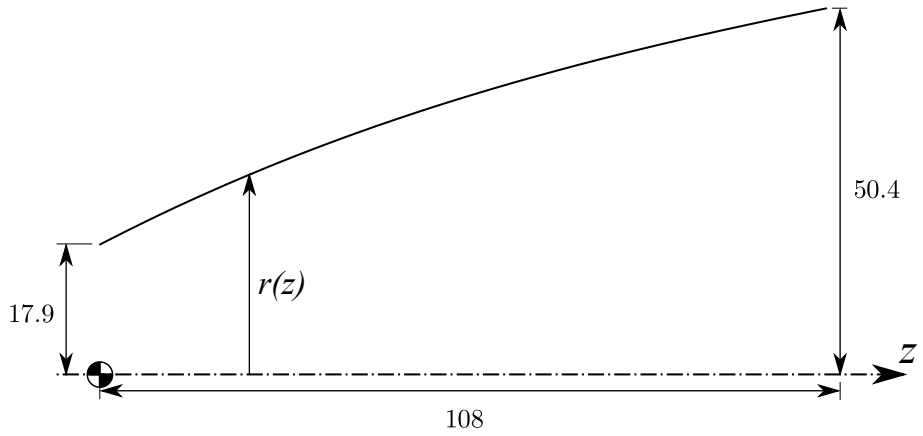

Figure 14: Generatrix of a non-cylindrical mandrel - eq. (31).

It is important to notice that due to the nature of RK4, no corrective numerical procedure is employed. The objective herein is just to describe non-geodesic trajectories and, through the results, to present properties of these paths. To implement such winding type, one requires to apply some corrective control to the process in order to avoid the propagation / accumulation of errors [19].

4.3 Influence of the returning path on the pattern generation

In this section, the pattern generation and non-geodesic trajectory will be used to define the dwell angle to produce a covered surface for a particular pattern. To define the procedure to obtain the most suitable dwell for the geometric approach, let's consider the wound component length $L = 181.4$ mm and pitch $L_r = 90.7$ mm ($\alpha = 60°$). It is also considered $p_{tr} = 5$ (as Section 2.3) and the slippage coefficient is 0.3. As depicted in Figure 11, the minimum dwell in this case is approximately $210°$. Given the possible choices presented in Table 1, the best condition in terms of manufacturing parameters is $s_{kp} = 1$, which gives a dwell of $216°$. A $p_{tr}/s_{kp} = 5/2$ is also possible. However, on each return manoeuvre, instead of the additional $6°$ of the case of $p_{tr}/s_{kp} = 5/1$, the necessary dwell is $222°$, increasing manufacturing costs and time.

Now, for $L = 200$ mm, $\alpha = 60°$ and $p_{tr} = 5$, the pitch does not fit exactly the component length $\left(\frac{L}{L_r} \approx 2.2\right)$ and, thus, $a_l = 18.6$ mm. Then, the modified dwell (eq. (12)) and its relation with the pattern is

$$\hat{d}_w = 73.91 + d_w \Rightarrow 369.57 + 5d_w \equiv 0 \,(\mathrm{mod} 180) \tag{32}$$

The results of eq. (32) are summarised as

$$\begin{aligned} d_w^{(1)} &= 34.09° + 180°n \\ d_w^{(2)} &= 70.09° + 180°n \\ d_w^{(3)} &= 106.09° + 180°n \\ d_w^{(4)} &= 142.09° + 180°n \\ d_w^{(5)} &= 178.09° + 180°n \end{aligned} \tag{33}$$

where $n \in \mathbb{N} \cup \{0\}$. The solutions of eq. (33) are related to the minimum possible dwell for a particular slippage coefficient. Considering four different λ, as shown in Figure 11, different dwells are calculated as shown in Table 6. One observes that for $\lambda = 0.1$ and $\min \hat{d}_w = 649.09°$, the generated pattern falls in the case of $1/1$, the dwell in both ends is multiple of $360°$. In this case, a pattern of $5/1$ is achievable with $\hat{d}_w = 682.09°$.

Table 6: Evaluations of the dwell regarding the slippage coefficient

λ	$\min \theta$	$\min \hat{d}_w$ (eq. 33)	p_{tr}/s_{kp}
0.1	$629.44°$	$646.09°$	$1/1$
0.2	$314.72°$	$322.09°$	$5/1$
0.3	$209.82°$	$214.09°$	$5/3$
0.4	$157.36°$	$178.09°$	$5/2$

4.4 Evaluating the possible patterns and manufacturing variables

In this section, the step-by-step methodology for obtaining all manufacturing parameters are shown for a few simple examples. Considering the design through the methodology herein proposed for a cylinder with $L = 450.6$ [mm] and $r = 30$ [mm]. The tow width is set as $w = 3.5$ [mm] and the desired winding angle is $60°$. In order to analyze the influence of the slippage coefficient, two values are used $\lambda = 0.1$ and $\lambda = 0.3$. Furthermore, a minimum mandrel length (encompassing the regular winding and return regions) as well as a minimum superposition of tows that covers all the periphery of the mandrel are sought. In other words, for the last, the degree of coverage must be larger than 100%.

A schematic flowchart is presented in Figure 15 showing the correlation between variables.

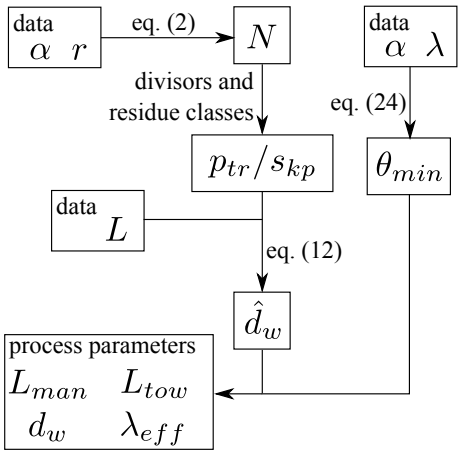

Figure 15: Procedure Flowchart.

It is relatively simple, by considering the minimum superposition possible, to define the number of tows and degree of coverage: $N = 27$ and 100.3 %, respectively. Then, with eq. (2) and $a = 1$, the possible patterns are

$$p_{tr} = \{1 \quad 3 \quad 9\} \tag{34}$$

and the p_{tr}/s_{kp} sets, through the residue classes, are defined as

$$\begin{aligned} &p_{tr} = 1 \rightarrow p_{tr}/s_{kp} = \{1/1\} \\ &p_{tr} = 3 \rightarrow p_{tr}/s_{kp} = \{3/1 \;\; 3/2\} \\ &p_{tr} = 9 \rightarrow p_{tr}/s_{kp} = \{9/1 \;\; 9/2 \;\; 9/4 \;\; 9/5 \;\; 9/7 \;\; 9/8\} \end{aligned} \tag{35}$$

in which the patterns ($3/3$ or $9/3$, for example) that fall into another one are already eliminated from the sets.

Now, the dwells for each pattern is then obtained by modular arithmetic. Then, for each case in eq. (35), the required

d_w is

$$
\begin{aligned}
p_{tr} = 1 \quad s_{kp} = 1 \quad &\rightarrow \quad d_w = 129.4272 + 180n \\
p_{tr} = 3 \quad s_{kp} = 1 \quad &\rightarrow \quad d_w = 9.4272 + 180n \\
s_{kp} = 2 \quad &\rightarrow \quad d_w = 69.4272 + 180n \\
p_{tr} = 9 \quad s_{kp} = 7 \quad &\rightarrow \quad d_w = 89.4272 + 180n \\
s_{kp} = 8 \quad &\rightarrow \quad d_w = 109.4272 + 180n \\
s_{kp} = 1 \quad &\rightarrow \quad d_w = 149.4272 + 180n \\
s_{kp} = 2 \quad &\rightarrow \quad d_w = 169.4272 + 180n \\
s_{kp} = 4 \quad &\rightarrow \quad d_w = 29.4272 + 180n \\
s_{kp} = 5 \quad &\rightarrow \quad d_w = 49.4272 + 180n
\end{aligned}
$$

noticing that the skip is obtained by applying each $\hat{d}_w$ into the eq. (3).

Parallel to these definitions, there exists the mechanical part of the process. Through it, one obtains the bounds for the return region – the minimum dwell. Let one consider first $\lambda = 0.1$. The mandrel requires to turn, at least, $629.4585°$ so that the tow remains in the predicted trajectory: dwells greater than this values requires friction lower than the available and *vice-versa*. So, Table 7 presents some results compilation of the methodology herein presented, where λ_{eff}, L_{tow} and L_{man} correspond to the effective slippage coefficient (the one required for the non-geodesic path), length of the tow and the mandrel's additional length for the returning process.

Table 7: Properties of the FW process for $\lambda = 0.1$

p_{tr}/s_{kp}	d_w [°]	λ_{eff} [adm]	L_{tow} [mm]	L_{man} [mm]
$1/1$	$669.4272°$	0.0940	184.20	49.36
$3/1$	$729.4272°$	0.0863	200.71	53.78
$3/2$	$789.4272°$	0.0797	217.22	58.20
$9/1$	$689.4272°$	0.0913	189.71	50.83
$9/2$	$709.4272°$	0.0887	195.21	52.31
$9/4$	$749.4272°$	0.0840	206.22	55.26
$9/5$	$769.4272°$	0.0818	211.72	56.73
$9/7$	$809.4272°$	0.0778	222.73	59.68
$9/8$*	$649.4272°$	0.0969	178.70	47.88

By considering uniquely the material quantity, the pattern $9/8$ would be the best choice, given it has the smallest L_{tow} and, consequently, the smallest L_{man}. The mandrel's size should be, for this case, 546.36 [mm] at least. Moreover, this case uses most of the friction available ($\approx 97\%$). The worst case is the pattern $9/7$ – the mandrel's size would be 569.96 [mm].

One considers the same parameters but $\lambda = 0.3$. A similar table is then assembled. For this case, the minimum dwell is $209.82°$. The best configuration for this slippage coefficient is $p_{tr}/s_{kp} = 9/5$, as shown in Table 8, while the worst is $9/4$. The percentile difference between the length of the tow of the aforementioned cases is $\approx 60\%$. Not to mention that the mandrel of the worst case requires to be much greater than the best (28.71 mm to 16.92 mm at the returning region).

Tables 7 and 8 shows that the slippage coefficient changes the optimum p_{tr}/s_{kp}, regarding uniquely the material waste and the mandrel's size. If other variables are considered – such as mechanical behaviour of the wound component, one may have the support of the flowchart on Figure 15 so as to evaluate p_{tr}/s_{kp} concerning small variations of parameters such as tow width, radius, etc., in order to obtain both good mechanical and process performances.

Table 8: Properties of the FW process for $\lambda = 0.3$

p_{tr}/s_{kp}	d_w [°]	λ_{eff} [adm]	L_{tow} [mm]	L_{man} [mm]
$1/1$	$309.4272°$	0.2034	85.14	22.81
$3/1$	$369.4272°$	0.1704	101.65	27.24
$3/2$	$249.4272°$	0.2524	68.63	18.39
$9/1$	$329.4272°$	0.1910	90.65	24.29
$9/2$	$349.4272°$	0.1801	96.15	25.76
$9/4$	$389.4272°$	0.1616	107.16	28.71
$9/5$*	$229.4272°$	0.2744	63.13	16.92
$9/7$	$269.4272°$	0.2336	74.14	19.86
$9/8$	$289.4272°$	0.2175	79.64	21.34

5 Conclusions

This article has introduced a novel proposal for pattern generation applied to FW process. It is based on the sequence of movements and geometric aspects of the process. A mathematical description of the process is formulated considering modular arithmetic, including main properties and developed mandrel's surface. Differences between the usual methodology (based on Diophantine equations) and the one introduced herein are also discussed. Two cases are analysed in detail: when the number of pitches fits exactly the winding region and when it does not. The possible patterns are obtained in a simpler way in comparison to the usual method, and the required dwell for a particular pattern/skip follows an elegant modular equation. This approach can also be implemented in CAM software along with the Diophantine equations in order to provide the designer with more alternatives for wound cylinders.

The methodology allows the best dwell for a given pattern and the influence of the slippage coefficient on the return trajectory for both cylindrical and non-cylindrical surfaces of revolution. The possible patterns for a particular mandrel's radius, winding angle and tow width configurations are defined. Results of a routine developed in a CAE software utilising this methodology are included.

The influence of the slippage coefficient on the dwell angle and additional mandrel's length for the return manoeuvre is studied for cylindrical and non-cylindrical surfaces. The influence initial winding angle given a slippage coefficient was also investigated, both for the dwell and the additional mandrel's length.

The winding angle variation and the mandrel's rotation angle for non-cylindrical surfaces of revolution were examined as well. The problem of finding the best dwell for a given a pattern was analysed, and the skip choice for a particular manufacturing case was discussed. So, as presented, the pattern (and the skip) can modify greatly the process efficiency – in terms of material waste and time of process – and the introduced methodology eases the achievement of such pattern / skip.

Acknowledgements

The authors would like to thank CAPES (project nos. 1303477 and 88881.198774/2018-1), CNPq (project nos. 310649 and 424426/2016-1), FAPERGS (project no. 17/2551-0001188-0) and, DAAD (project no. 57447163) for financial support.

Appendix A - Determination of the relation between the pattern and dwell

Let insert eq. (9) into eq. (11). It results in

$$2p_{tr}\left(360\left\lfloor\frac{L}{L_r}\right\rfloor+\hat{d}_w\right)\equiv 0\pmod{360}$$
$$2p_{tr}360\left\lfloor\frac{L}{L_r}\right\rfloor+2p_{tr}\hat{d}_w\equiv 0\pmod{360}$$

By the same rule that infers the reduction of the pattern given a skip, one obtains

$$p_{tr}360\left\lfloor\frac{L}{L_r}\right\rfloor+p_{tr}\hat{d}_w\equiv 0\pmod{180}$$

This simplification is possible given the symmetry of the strokes inside a circuit. And due to the properties of sum in modular arithmetic: the value $p_{tr}360\left\lfloor\frac{L}{L_r}\right\rfloor$ belongs to the residue class $[0]_{180}$ as $p_{tr}\in\mathbb{N}\setminus 0$ and $\left\lfloor\frac{L}{L_r}\right\rfloor\in\mathbb{N}$ and, therefore, $p_{tr}\left\lfloor\frac{L}{L_r}\right\rfloor\in\mathbb{N}$. Any non-negative integer multiplied by 360 belongs to the residue class $[0]_{180}$. This proves that the region of regular winding with geodesic trajectory have influence of any kind in the pattern generation. Then

$$[0]+p_{tr}\hat{d}_w\equiv p_{tr}\hat{d}_w\equiv 0\pmod{180}$$

in which is the eq. (12).

References

[1] B. S. Johansen, A. Lystrup, and M.T. Jensen. Cadpath: a complete program for the cad-, cae- and cam-winding of advanced fibre composites. Journal of Materials Processing Technology, 77(1–3):194–200, 1998.

[2] D. Trajkovski. Kinematic analysis of trajectory generation algorithms for filament winding machines. In Proceedings of 11th World Congress in Mechanism and Machine Science, August 2003.

[3] L. Zu, Q. X. He, and Q. Q. Ni. Pattern design for non-geodesic winding toroidal pressure vessels. In Proceedings of 16th International Conference on Composite Materials, July 2007.

[4] J. Sun and Q. Xiao. Study on winding pattern and undulation degree of filament-wound composite tube. Advanced Materials Research, 341–342:281–285, 2012.

[5] L. Sorrentino, W. Polini, L. Carrino, E. Anamateros, and G. Paris. Robotized filament winding of full section parts: Comparison between two winding trajectory planning rules. Advanced Composite Materials, 17(1):1—-23, 2008.

[6] J. Rousseau, D. Perreux, and N.Verdière. The influence of winding patterns on the damage behaviour of filament-wound pipes. Composites Science and Technology, 59(9):1439–1449, 1999.

[7] E. Morozov. The effect of filament-winding mosaic patterns on the strength of thin walled composite shells. Composite Structures, 76(1–2):123–129, 2006.

[8] A. M. Zakrzhevskii and V. V. Khitrov. Effect of interweaving on the load-carrying capacity of wound thick-walled rods of composites in torsion. Mechanics of Composite Materials, 24(4):516–523, 1989.

[9] H. Hahn, D. W. Jensen, S. J. Claus, S. Pai, and P. A. Hipp. Structural design criteria for filament wound composite shells. NASA Technical Reports, University Park, 1995.

[10] H. Hernández-Moreno, B. Douchin, F. Collombet, D. Choqueuse, and P. Davies. Influence of winding pattern on the mechanical behavior of filament wound composite cylinders under external pressure. Composites Science and Technology, 68(3–4):1015–1024, 2008.

[11] S. Koussios. Filament Winding - A Unified Approach. IOS Press, 2004.

[12] A. Beukers, S. Koussios, and O. Bergsma. Composite pressure vessel design: integral determination of winding patterns. In Proceedings of 16th International Conference on Composite Materials, July 2007.

[13] P. A. Lowery. Continued fractions and the derivation of uniform-coverage filament winding patterns. SAMPE Journal, 26(5):57–64, 1990.

[14] Y. D. Liang and G. Luo. A simple filament winding pattern generation algorithm. International Smape Technical Conference, 28:1027–1039, 1996.

[15] J. M. Dolan, P. Khosla, and S. Talukdar. Surface-closure algorithms for filament winding of non-axisymmetric cylindrical parts. In Proceedings of the 25th International SAMPE Technical Conference, pages 680–691, October 1993.

[16] I. Niven, H. Zuckermann, and H. Montgomery. An Introduction to the Theory of Numbers. John Wiley & Sons, Inc., New York, 1991.

[17] V. V. Vasiliev. Composite Pressure Vessels: Analysis, Design and Manufacturing. Bull Rigde Publishing, Blacksbury, 2009.

[18] A. Gray. Modern differential geometry of curves and surfaces. CRC Press, Inc., Boca Raton, 1993.

[19] S. T. Peters. Composite Filament Winding. ASM International, Materials Park, 2011.

[20] L. Zu, S. Koussios, and A. Beukers. Design of filament-wound isotensoid pressure vessels with unequal polar openings. Composite Structures, 92(9):2307–2313, 2010.